Density Functional Theory Study of the Mechanisms of Iron-Catalyzed Cross-Coupling Reactions of Alkyl Grignard Reagents

ARTICLE *in* THE JOURNAL OF PHYSICAL CHEMISTRY A · JANUARY 2013

Impact Factor: 2.69 · DOI: 10.1021/jp3045498 · Source: PubMed

4 AUTHORS:

Qinghua Ren
Shanghai University
29 PUBLICATIONS **222** CITATIONS
SEE PROFILE

Shu Hui Guan
Fudan University
4 PUBLICATIONS **11** CITATIONS
SEE PROFILE

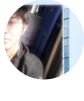

Jiang Feng
Leiden University
6 PUBLICATIONS **41** CITATIONS
SEE PROFILE

Jianhui Fang
Shanghai University
48 PUBLICATIONS **847** CITATIONS
SEE PROFILE

THE JOURNAL OF PHYSICAL CHEMISTRY A

Article

pubs.acs.org/JPCA

Density Functional Theory Study of the Mechanisms of Iron-Catalyzed Cross-Coupling Reactions of Alkyl Grignard Reagents

Qinghua Ren,* Shuhui Guan, Feng Jiang, and Jianhui Fang

Department of Chemistry, Shanghai University, 99 Shangda Road, Shanghai 200444, China

Supporting Information

ABSTRACT: When compared with the established palladium and nickel catalyst systems, simple iron salts turn out to be highly efficient, cheap, toxicologically benign, and environmentally friendly precatalysts for a host of cross-coupling reactions of alkyl or aryl Grignard reagents. The inorganic Grignard reagent [$Fe(MgX)_2$], where X corresponds to Br or I, is a good catalyst for cross-coupling reactions. The present study reports a thorough theoretical analysis of the mechanisms of the [$Fe(MgBr)_2$] catalyzed cross-coupling reaction between 4-chlorobenzoic acid methyl ester and *n*-hexylicmagnesium bromide using density functional theory (DFT) calculations. Our calculations show that the overall catalytic cycle includes three basic steps: oxidation of [$Fe(MgBr)_2$] to obtain [Ar−Fe(MgBr)], addition to yield [Ar−(*n*-hexyl)−$Fe(MgBr)_2$], and reductive elimination to return to [$Fe(MgBr)_2$]. The energy barrier is lower if *n*-hexylicmagnesium bromide attacks the intermediate of the oxidative addition directly before [Cl−Mg−Br] dissociates to form the middle product [Ar−Fe(MgBr)] than if the attack occurs after the dissociation of [Cl−Mg−Br]. The solvation effect in this step clearly leads to a lowering of the energy barrier. The rate-limiting step in the whole catalytic cycle is the reductive elimination of [Ar−(*n*-hexyl)−$Fe(MgBr)_2$] to regenerate the catalyst [$Fe(MgBr)_2$], where the electronic energy barrier ΔE is 29.74 kcal/mol in the gas phase and the Gibb's free energy in solvent THF ΔG_{sol} is 28.13 kcal/mol computed using the C-PCM method.

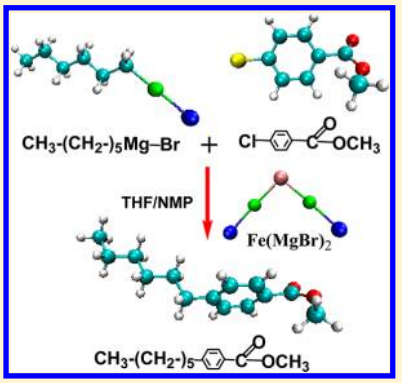

1. INTRODUCTION

The formation of carbon−carbon as well as carbon−heteroatom bonds by transition metal-catalyzed cross-coupling is of utmost importance for modern organic synthesis.[1−10] Palladium and nickel catalysts dominate this field because of their wide scope and excellent compatibility with many functional groups.[3,5,8,11−14] However, they are limited by the high price or considerable toxicity, especially in the context of manufacturing on larger scales. Furthermore, both palladium and nickel catalyst systems usually require the addition of structurally complex and costly ligands of high molecular weight. In order to improve the existing cross-coupling methodologies, iron-catalyzed carbon−carbon bond-forming reactions have started to be used and have over the past decade matured into an indispensable class of reactions because of their broad applicability, their high efficiency, cheapness, nontoxicity, and the environmental friendliness of the simple iron salt precatalysts.[15−18]

The iron-catalyzed cross-coupling reactions were originally proposed in 1971 by Kochi et al.[19,20] but did not attract much attention in the following decades, until the early 2000s when Furstner et al. reported a list of highly selective iron-catalyzed cross-coupling reactions of aryl halides with alkyl magnesium-halides.[21,22] Their work has stimulated a series of experimental publications[15,23−30] and the iron-catalyzed cross-coupling reactions have matured into a class of effective carbon−carbon and carbon−heteroatom bond-forming reactions with a wide substrate scope and functional group tolerances.

Ever since modern transition metal-catalyzed cross-coupling chemistry emerged in the 1970s,[4,31−33] much attention has been paid to the theoretical understanding of the reaction mechanisms of the prominent palladium-catalyzed and nickel-catalyzed processes. Computational studies have proven to be a useful tool for the mechanistic aspects of reactions, and many detailed theoretical studies of palladium-catalyzed[34−38] and nickel-catalyzed[39−44] reactions have recently been published. The mechanism of the Pd-catalyzed process was proved to be mainly the transformation between $Pd(0)L_n$ and Pd(II) complexes. Alvarez and co-workers[34] reported the open transmetalation mechanism for the Stille cross-coupling of vinyl bromide and vinyl triflate with trimethylvinylstannane catalyzed by $Pd(PMe_3)_2$, but they did not discuss the effect of the solvent. Li[36] studied the mechanism of oxidative addition of aryl halides to $Pd(PR_3)_2$ (R = Me, Et, etc.). Sugiyama[37] investigated the mechanism of Pd-catalyzed cross-coupling reaction between vinyl iodide and trimethylvinylsilane and clarified the reasons why fluoride anion accelerates the transmetalation process. The Ni-catalyzed cross-coupling process was also found to be the transformation between Ni(0) catalyst and Ni(II) complexes.[39−41] Li[39] reported a thorough theoretical analysis of Ni-catalyzed cross-coupling between aryl esters and arylboronic acids, and McCarren[40]

Received: May 10, 2012
Revised: January 6, 2013
Published: January 9, 2013

investigated the mechanism for Ni-catalyzed reductive couplings of alkynes with aldehydes.

However, the mechanisms of the iron-catalyzed reactions remain rather obscure. The early mechanistic studies of iron catalysis in the cross-coupling of alkenyl halides and Grignard reagents were carried out by Jay K. Kochi in 1976.[45] They reported that the mechanism of the cross-coupling process could be accommodated by an oxidative addition of 1-bromopropene to iron(I) followed by exchange with ethylmagnesium bromide and reductive elimination, where the iron(III) intermediates are formed. Then, in 1986, Takacs et al. studied iron(0)-catalyzed diene to olefin cross-coupling reaction,.[46] but the hypotheses that Fe(0) or Fe(+I) species constituted the catalytically relevant intermediates were rendered highly unlikely along with the advances of Grignard reagents.

It is now well-known that the inorganic Grignard reagent $[Fe(MgX)_2]$, where X = Br or I, plays an important role in the cross-coupling catalytic cycle.[17,18,47] $[Fe(MgX)_2]$ consists of two magnesium atoms and one iron center that are connected via two covalent intermetallic bonds. Because the conditions of their experiments closely mimic those of standard cross-coupling protocols, Furstner et al.[21,22] have given a mechanistic proposal for the iron-catalyzed cross-coupling reaction shown in Scheme 1, where the initial $[Fe(MgX)_2]$ is formed from $FeCl_2$ and RMgX. This mechanism was generally used to explain many of their experimental results.[22,25,27]

Scheme 1. Mechanistic Proposal for the Iron-Catalyzed Cross-Coupling Reaction

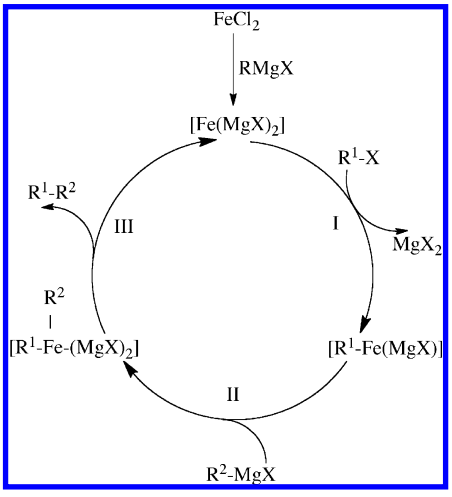

Here the iron center is Fe(-II) in $[Fe(MgX)_2]$, and Fe(0) in $[R_1-Fe(MgX)]$ and $[R_1-(R_2)-Fe(MgX)_2]$. The Fe(-II) and Fe(0) catalytic cycle is different from the generally accepted Pd(0) and Pd(II) catalytic cycle or Ni(0) and Ni (II) catalytic cycle. Recently Norrby[48] reported an investigation of a mechanism similar to that proposed by Kochi.[19,20,45] The rate-limiting step is an oxidative addition of an iron complex in the Fe(I) oxidation state to the aryl substrate. However, to the best of our knowledge, detailed theoretical studies concerning the $[Fe(MgX)_2]$ catalyzed cross coupling processes have not as yet been performed. Furthermore, many experimental results involving iron-catalyzed cross-coupling of alkyl or aryl Grignard reagents have recently been reported.[49−51] But none of these studies have investigated the mechanisms of the reactions. An understanding of the detailed mechanisms of iron-catalyzed cross-coupling reactions will shed light on how to design more powerful iron-salt catalysts and how to control the catalysis process. It is therefore useful to perform further computational studies on the mechanism of these reactions especially when the direct spectroscopic investigations of the actual intermediates involved in the formal catalytic cycle outlined above are hampered by various factors.

Here, we select one typical reaction in the experimental work of Furstner[22] as an example in order to gain insight into the mechanisms of iron-catalyzed cross-coupling reactions. Our thorough theoretical investigation is applied to $[Fe(MgBr)_2]$ catalyzed cross-coupling reaction between 4-chlorobenzoic acid methyl ester [Cl−Ph−COOMe] and *n*-hexylicmagnesium bromide [*n*-$CH_3(CH_2)_5$−MgBr] using density functional theory (DFT) calculations with the B3LYP method.[52−57]

The experimental result[22] for the system in question is depicted in Scheme 2, where the yield was 91% and the reaction was carried out in THF/NMP using $Fe(acac)_3$ (5 Mol %) as the precatalyst because it is cheap and nonhygroscopic but equally effective as $FeCl_2$. $Fe(acac)_3$ reacts with R-MgBr to yield the inorganic Grignard reagent $[Fe(MgBr)_2]$, which is readily soluble in ethereal solvents such as THF. Our theoretical studies start from the catalyst $[Fe(MgBr)_2]$, which catalyzes the cross-coupling reaction. Our calculations will examine these questions: Whether the overall catalytic cycle includes three basic steps: (I) oxidation of $[Fe(MgBr)_2]$ to obtain [Ar−Fe(MgBr)], (II) addition to yield [Ar−(*n*-hexyl)−$Fe(MgBr)_2$], and (III) reductive elimination to return to $[Fe(MgBr)_2]$ (see Scheme 1) . Which step is rate determining in the whole catalytic cycle? Is it possible to lower the energy barrier if the solvent effect is considered? Answers to these questions will improve the understanding of iron-catalyzed cross-coupling of Grignard reagents.

Scheme 2. Iron-Catalyzed Cross-Coupling Reaction between 4-Chlorobenzoic Acid Methyl Ester and *n*-Hexylicmagnesium Bromide

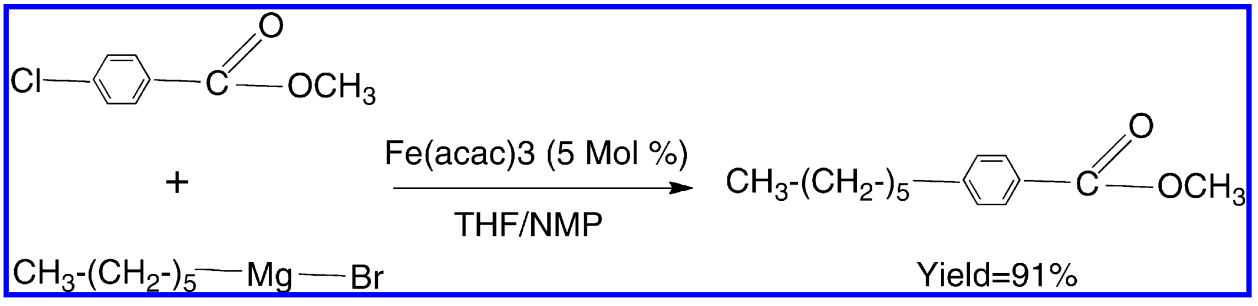

dx.doi.org/10.1021/jp3045498 | J. Phys. Chem. A 2013, 117, 756−764

2. COMPUTATIONAL METHODS

The quantum mechanical computations were performed using density functional theory (DFT) with the B3LYP hybrid functional[52−57] in conjunction with the 6-311++G(d,p) basis set,[58,59] on all nonmetal atoms and also Mg atom, and the SDD quasi-relativistic pseudopotential and associated basis set for iron.[60] All equilibrium structures of the gas phase geometries were fully optimized without any symmetry restriction, following the vibrational frequencies analysis to ensure that the local minima had zero imaginary frequencies and the transition state had exactly one. The values of electronic energy ΔE, zero-point energy correction ΔZPE, relative enthalpy ΔH, relative entropy ΔS, and Gibb's free energy ΔG (298 K) were calculated. The unit of the relative entropy ΔS is cal/(mol K) and all the other energy units are kcal/mol.

The solvation effect was calculated using the C-PCM polarizable conductor calculation model[61] with the UFF radii on the gas-phase optimized geometries of single points. Both the electronic and nonelectronic free energies in solution were added to the gas-phase Gibbs free energies to obtain the solution Gibbs free energies in THF, ΔG_{sol}. All the solution-phase free energies reported in the article correspond to the reference state of 1 mol/L, 298 K. All calculations were performed using the Gaussian03 program.[62]

3. RESULTS AND DISCUSSION

3.1. Full Catalytic Cycle. The whole catalytic cycle explored is outlined in Figure 1, which includes three transition

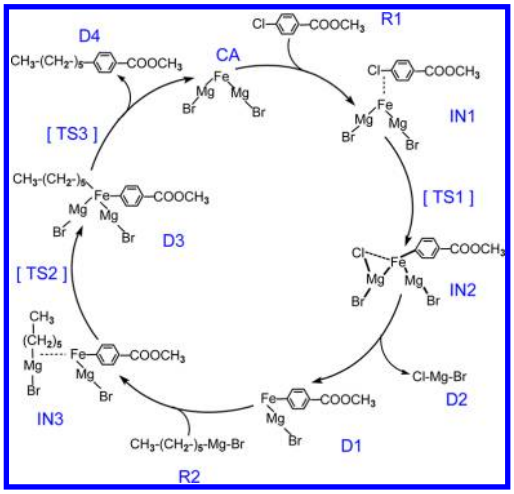

Figure 1. Outline of the iron-catalyzed cross-coupling reaction mechanism for the product **D4** from **R1** and **R2**.

states (**TS1**, **TS2**, and **TS3**). The fully optimized structures of reactants (**R1** and **R2**), the catalyst (**CA**), the η^2-complex (**IN1**), the transition state (**TS1**), the intermediate (**IN2**), the middle product (**D1**), and the final product (**D2**) are shown in Figure 2. The full optimized geometries of the η^2-complex (**IN3**), the transition states (**TS2** and **TS3**), the middle product (**D3**), and the final product (**D4**) are shown in Figure 3. The values of the important bonding distances are also given in Figures 2 and 3 (distances are given in Å). The products **D1**, **D3**, **D2**, and **D4** correspond to $[R^1-Fe(MgX)]$, $[R^1-(R^2-)Fe-(MgX)_2]$, MgX_2, and $[R^1-R^2]$ shown in Scheme 1.

The mechanism is similar as the mechanistic proposal given by Furstner et al.[21,22] shown in Scheme 1, which includes three basic steps: (I) Oxidation of $[Fe(MgBr)_2]$ to obtain $[Ar-Fe(MgBr)]$. The approach of **R1** toward the catalyst **CA**, $[Fe(MgBr)_2]$, leads to the formation of an η^2-complex **IN1** (see its optimized structure in Figure 2). From **IN1**, a three-membered-ring transition state **TS1** is identified. The intermediate of oxidative addition is **IN2**. In the optimized geometry of **TS1**, the chlorine atom approaches toward Mg_2 atom around the iron center departing from C_1 atom. The separation of Cl−Fe is 2.39 Å. It becomes 2.30 Å in the optimized geometry of **IN2**, accompanying with the formation of Cl−Mg_2 bond (see Figure 2). Because of the bonding of the Cl atom with the Mg_2 atom and the interaction of the Cl atom with an Fe atom, the separation of Fe−Mg_2 increases to 2.62 Å in the optimized structure of **IN2**. The weakening process of the bonding of Fe−Mg_2 is beneficial for the further reaction, i.e., the covalent intermetallic bonding of Fe−Mg_2 breaks and the molecule **D2** dissociates to form the middle product **D1**, $[(BrMg)-Fe-(Ph-COOCH_3)]$.

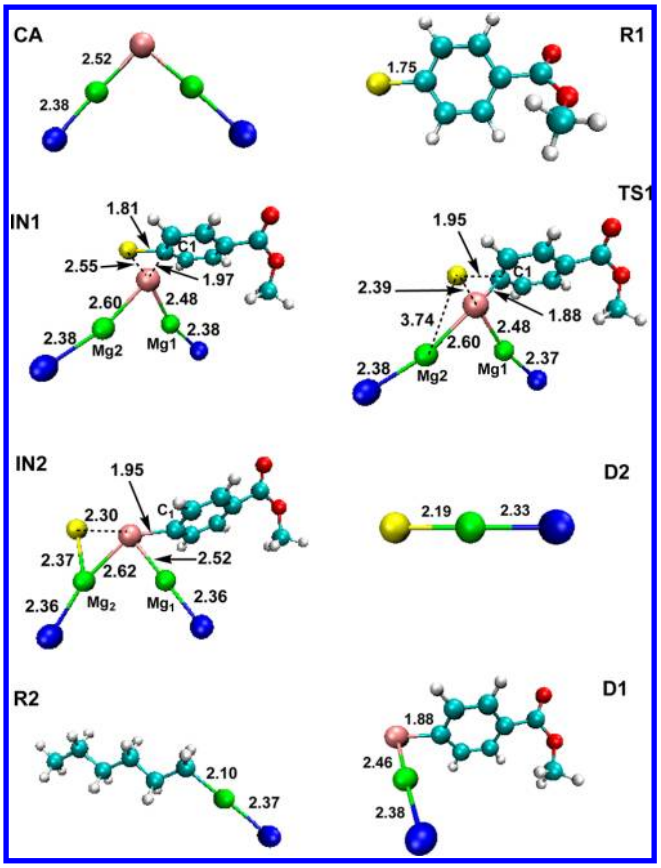

Figure 2. Fully optimized structures of the reactants, **R1** and **R2**, the catalyst, **CA**, the intermediates, **IN1** and **IN2**, the transition state, **TS1**, the middle product, **D1**, and the final product, **D2**. The unit of the distance is Å (C, cyan; O, red; Fe, pink; Mg, green; Br, blue; Cl, yellow).

(II) Addition of another reactant **R2** to **D1** yields the second middle product **D3**, $[Ar-(n\text{-hexyl}-)-Fe(MgBr)_2]$. After the middle product **D1** is formed, the approach of **R2** toward **D1** leads to the formation of an η^2-complex **IN3**. From **IN3**, passing through a three-membered-ring transition state **TS2**, the middle product **D3** is formed. The fully optimized structures of **IN3**, **TS2**, and **D3** are shown in Figure 3. It can be seen that the Fe−Mg_2 distance is 2.57 Å in **TS2**, compared to that of 2.73 Å in **IN3**. The separation of Fe−C_2 also decreases from 3.35 Å in **IN3** to 3.01 Å in **TS2**, so that it is easy

dx.doi.org/10.1021/jp3045498 | J. Phys. Chem. A 2013, 117, 756−764

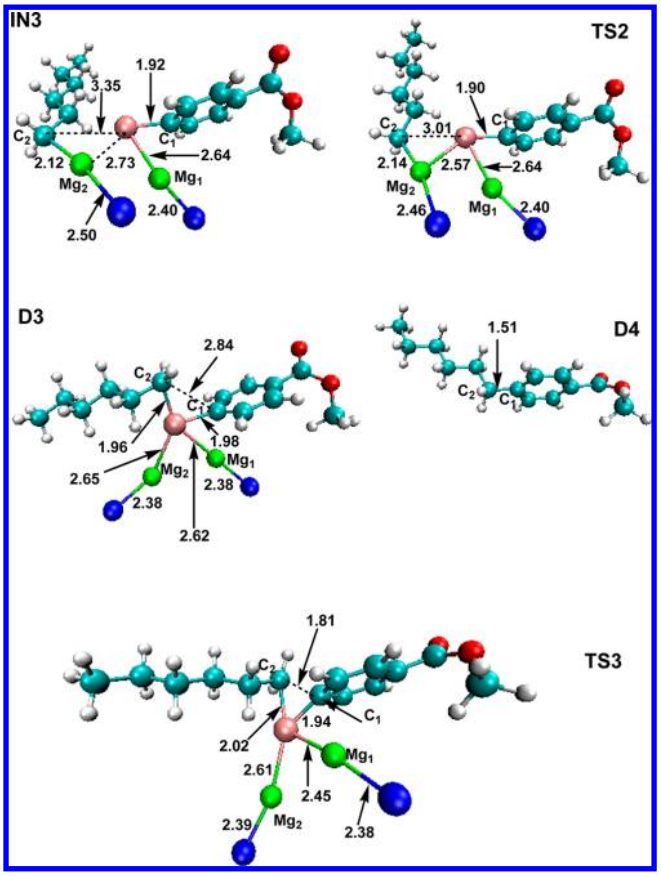

Figure 3. Fully optimized structures of the intermediate, **IN3**, the transition states, **TS2** and **TS3**, the middle product, **D3**, and the final product, **D4**. The unit of the distance is Å (C, cyan; O, red; Fe, pink; Mg, green; Br, blue; Cl, yellow).

for atom C_2 to attack the Fe atom in **TS2**, leading to the formation of a Fe−C_2 bond to obtain the middle product **D3**.

(III) Finally, reductive elimination of **D3** returns the catalyst **CA**, [Fe$(MgBr)_2$]. This process passes through the third transition state **TS3** to form the final product **D4**, [*n*-$CH_3(CH_2)_5$−Ph−$COOCH_3$] and to regenerate the original catalyst **CA**. The fully optimized structures of **TS3** and **D4** are also shown in Figure 3.

3.2. Energy Profile. The electronic energy profile for the overall catalytic cycle of the iron-catalyzed cross-coupling reaction between 4-chlorobenzoic acid methyl ester [Cl−Ph−$COOCH_3$] and *n*-hexylicmagnesium bromide [*n*-$CH_3(CH_2)_5$−MgBr] is depicted in Figure 4, where the summation of the electronic energies of the reactant **R1** and the catalyst **CA** is set as zero energy.

From the values in Figure 4, we can see that the process in which the molecule **D2**, [Cl−Mg−Br], dissociates from the intermediate **IN2** to form the middle product **D1** is endothermic by +35.91 kcal/mol. It refers to the breaking of the strong covalent intermetallic bonding of Mg−Fe. This could be offset by the large exothermicity (−70.50 kcal/mol) process forming the intermediate **IN2** from **IN1**. The transition state connecting **IN2** and **D1** has not been found after many attempts. The energy barrier of **TS3** to form the final product **D4** from the middle product **D3** when releasing the catalyst **CA** through the reductive elimination is +29.74 kcal/mol. This process is needed to break two Fe−C bonds. These two steps (i.e., **IN2** → **D1** and **D3** → **CA** + **D4**) are the rate-limiting

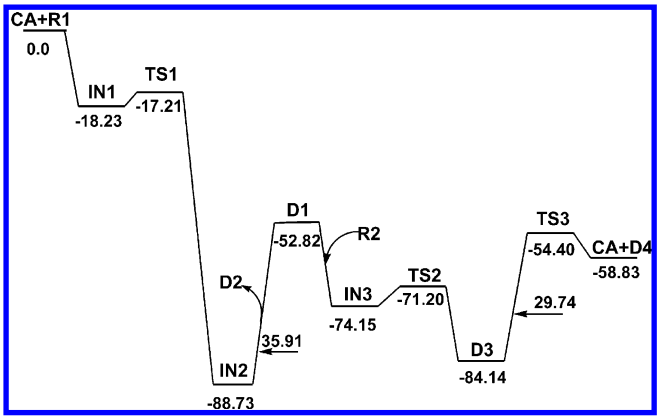

Figure 4. Electronic energy profile for the overall catalytic cycle of the iron-catalyzed cross-coupling reaction (energies quoted in kcal/mol).

steps in the catalytic cycle. The energy profile from η^2-complex **IN1** to the first transition state **TS1** is small (+1.02 kcal/mol). The energy barrier of **TS2** from **IN3** to form a stable structure **D3** [R^1−(R^2−)Fe−$(MgBr)_2$] is also small (+2.95 kcal/mol).

3.3. Other Path without Forming [Ar−Fe(MgBr)]. In view of the fact that the required electronic energy for the process in which the molecule **D2**, [Cl−Mg−Br] dissociates from the intermediate **IN2** to form the middle product **D1** is very high by +35.91 kcal/mol (see Figure 4), it could be possible that there is another way to lower the energy barrier, namely if *n*-hexylicmagnesium bromide (**R2**) attacks the intermediate **IN2** directly before the formation of **D1** [Ar−Fe(MgBr)]. Our calculations have proved that this new path is easier than the previous catalytic cycle shown in Figure 1, as proposed by Furstner.[21,22] The electronic energy profile from the intermediate **IN2** to the middle product **D3** for the new path is depicted in Figure 5.

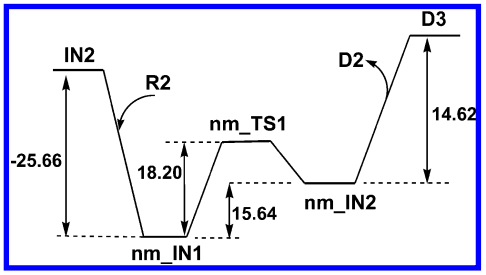

Figure 5. Electronic energy profile (energies given in kcal/mol) for the new cycle of the reaction mechanism from **IN2** to **D3**.

From Figure 5, we can see that the reactant **R2** first approaches toward the intermediate **IN2** to form **nm_IN1**. From **nm_IN1**, after passing through one transition state **nm_TS1**, an intermediate **nm_IN2** is formed, where the fully optimized structures of **nm_IN1**, **nm_TS1**, and **nm_IN2** in the gas phase are shown in Figure 6. Then, the molecule **D2** dissociates from the intermediate **nm_IN2** to yield **D3**. In the optimized geometry of **nm_IN1**, the bonding of Cl−Mg_3 is nearly formed (2.47 Å), and the Fe−Br_3 distance is 2.49 Å. The Cl−Mg_2 bond length becomes longer and reaches 2.64 Å compared to that of 2.37 Å in **IN2**, which means the Cl atom is now linked to the Mg_3 atom. The distance of Cl with Fe also becomes longer to 2.39 Å, compared to that of 2.30 Å in **IN2**. Next, the atom Br_3 in **nm_IN1** rotates around the Mg_3 atom to bring the atom C_2 close to the Fe atom, so that the atom C_2 can

dx.doi.org/10.1021/jp3045498 | J. Phys. Chem. A 2013, 117, 756−764

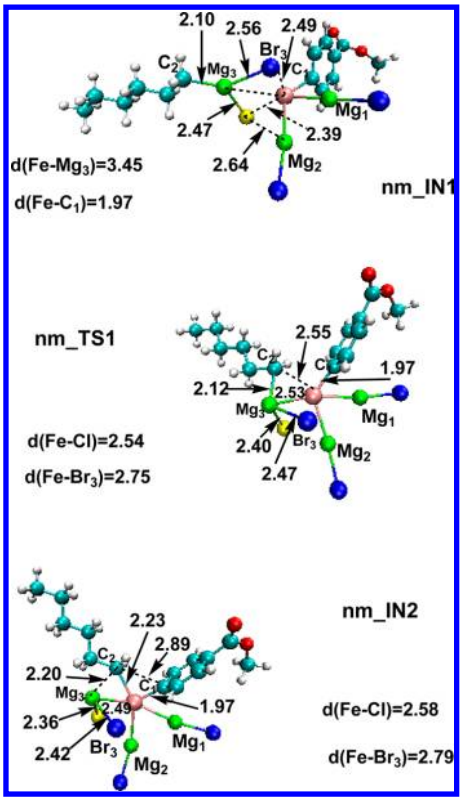

Figure 6. Fully optimized structures of the intermediates, **nm_IN1** and **nm_IN2**, and transition state, **nm_TS1**, for the new mechanism. The unit of the distances is Å (C, cyan; O, red; Fe, pink; Mg, green; Br, blue; Cl, yellow).

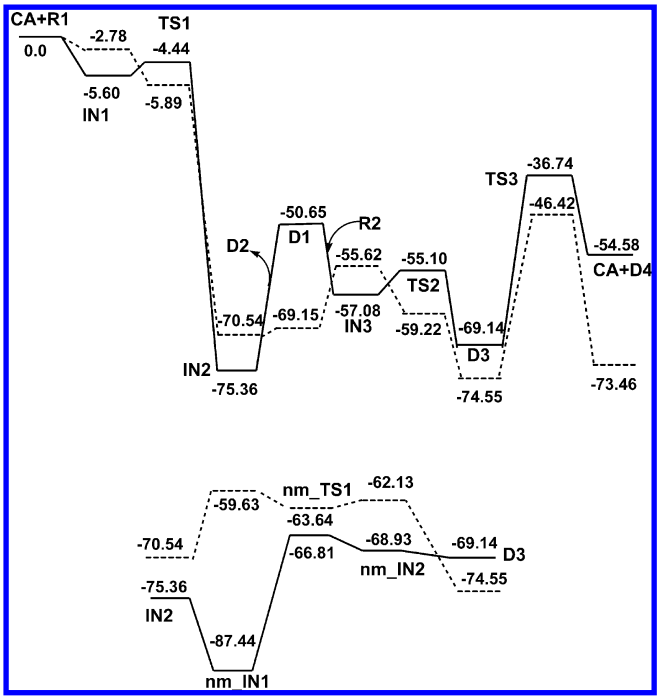

Figure 7. Gibb's free energy ΔG in gas phase (solid line) and Gibb's free energies in THF solution ΔG_{sol} (298 K) (dashed line) for the overall catalytic cycle (energies are quoted in kcal/mol).

attack the Fe center easily. In the optimized structure of the transition state **nm_TS1**, the distance of atom C_2 from the Fe atom is 2.55 Å. It becomes shorter to 2.23 Å in the optimized structure of **nm_IN2**, which is close to the value of 1.96 Å in the optimized structure of **D3** (see Figure 3).

It can be seen from Figure 5 that the electronic energy barrier to pass over the transitional state **nm_TS1** is only 18.20 kcal/mol, which is much smaller than the +35.91 kcal/mol required when the molecule **D2**, [Cl−Mg−Br], dissociates directly from the intermediate **IN2** before another reactant **R2** attacks. So this new path should be more easily realized.

From the whole catalytic cycle through the new path with **nm_IN1** and **nm_IN2**, it can be seen that the iron center is Fe(-II) in $[Fe(MgBr)_2]$, but Fe(0) in **IN1**, **IN2**, **nm_IN1**, **nm_IN2**, and **D3**. This Fe(-II) and Fe(0) catalytic cycle is different from the generally accepted Pd(0) and Pd(II) catalytic cycle.[34−36]

3.4. Solvation Effect Calculated Using the C-PCM Model. On the basis of the computational methods described in section 2, the calculated values of ΔE, ΔZPE, ΔH, ΔS, ΔG, and ΔG_{sol} are listed in Table S1 in the Supporting Information. In order to clarify the solvent effect clearly, we compare the Gibb's free energies ΔG and the Gibb's free energies in THF solution, ΔG_{sol}, for the overall catalytic cycle in Figure 7. The former is depicted as the solid line and the latter is drawn as the dashed line.

From Figure 7, it can be seen that the solvation effect is obvious for the step of dissociating **D2** from **IN2** to form **D1**, where ΔG_{sol} (**IN2** → **D1**) is 1.39 kcal/mol, which is much lower than ΔG (**IN2** → **D1**) in the gas phase (24.71 kcal/mol). Similarly, the solvation effect is also large for the step in which the final product **D4** is formed from **D3** through the reductive elimination of **CA**. The ΔG_{sol} (**D3** → **D4**) is 1.09 kcal/mol, compared to ΔG (**D3** → **D4**) in the gas phase (14.56 kcal/mol). These variations can be clearly seen in Figure 7.

In the reaction field model using PCM method, the solute is placed in a cavity in the solvent. The calculations of the surface charges of the solute and their interactions with the solvent lead to the free energy of solvation.[63] Generally, the solvent effect will be large for the dissociation processes, which can be attributed to the fact that gas phase calculations strongly favor the formation of clusters and make dissociation reactions more difficult than in condensed phases.[63−65] Other calculations reported by Papai[66] also showed that the solvent effect is large for the process of dissociation of a PMe_3 ligand in the C−C coupling.

The solvent effect causes large changes of the ΔG values for the processes of (**IN2** → **D1**) and (**D3** → **D4**), where the solvation effect is exothermic. However, ΔG_{sol} (**D1** → **IN3**) for the process of forming **IN3** with the approach of **R2** toward **D1** is 13.53 kcal/mol, compared to ΔG= −6.43 kcal/mol of the gas phase value. The solvation effect is, in this case, endothermic. The solvation effects for other processes are not significant.

For another path without forming **D1**, [Ar−Fe(MgBr)], the value of Gibb's free energy in the gas phase ΔG_g (**nm_IN1** → **nm_TS1**) is 20.63 kcal/mol, but the value of Gibb's free energy in the THF solvent, ΔG_{sol} (**nm_IN1** → **nm_TS1**), is −4.01 kcal/mol. The salvation effect is obvious. The values of Gibb's free energies in the gas phase, ΔG_g, and in the THF solvent, ΔG_{sol}, for the step of (**nm_IN2** → **D3**), in which the molecule **D2** dissociates from the intermediate **nm_IN2** to yield **D3**, are very small, i.e., −0.21 kcal/mol and −12.42 kcal/mol, respectively. It is safe to assume that the energy barrier for the dissociation step is low in the overall cross-coupling process.[39]

dx.doi.org/10.1021/jp3045498 | J. Phys. Chem. A 2013, 117, 756−764

From Figure 7, it can also be seen that the new path involving **nm_IN1** and **nm_IN2** is favored over the path involving the formation of **D1** and **IN3** when in THF solution, where ΔG_{sol} (**IN2** → **nm_IN1**) = 10.91 kcal/mol is smaller than ΔG_{sol} (**D1** → **IN3**) = 13.53 kcal/mol. This conclusion is the same as that obtained from the gas phase calculations, where ΔG_g (**nm_IN1** → **nm_TS1**) = 20.63 kcal/mol is smaller than ΔG_g (**IN2** → **D1**) = 24.71 kcal/mol.

Now, the highest value of Gibb's free energy in THF solution for the whole cycle depicted in Figure 7 is the energy barrier of passing the transition state **TS3**, where ΔG_{sol} (**D3** → **TS3**) is 28.13 kcal/mol. This step in which the process of the reductive elimination of **D3** to form **D4** when the catalyst **CA** dissociates is the rate-limiting step of the catalytic cycle after considering the solvation effect.

3.5. Explicit Solvation Effect Calculated with Two Molecules of THF Included, Together with the C-PCM Method. Although the PCM method has been widely adopted in recent years in the description of the thermodynamic characteristics of solvation, it has the difficulty for the computation of free energy values for the dissociation of ligands that produce charged species mainly because of the large entropy effects in dissociation processes in the gas phase and the overestimation of the solvation energy of the resulting charged species.[34] For example, the PCM method greatly overestimates the solvation energy of Cl^-, leading to a solvation energy of 136 kcal/mol, compared with the estimated experimental value of 64 kcal/mol,[67] but for the system under investigation in this article, the solvent effect is large in both the process of (**IN2** → **D1**) where the molecule **D2**, [Cl−Mg−Br], dissociates and the process of (**D3** → **D4**) where the molecule **CA**, [Fe(MgBr)$_2$], dissociates. The dissociation products (**D2** + **D1** and **CA** + **D4**) are all neutral molecules. The calculations using C-PCM method should therefore not overestimate the solvation energy by too much.

In order to overcome the difficulty for the computation of the solvation energy of Cl^-, Shaik[68] checked that the solvation energy of $Cl^-(THF)^{7-10}$ embedded in PCM is 71 kcal/mol, which gets closer to the estimated experimental data. Thus, Shaik[69] suggested that a realistic solvation model that accounts for long-range interaction would have to involve more solvent (THF) molecules, but this kind of study for the entire catalytic cycle is too extensive at present.

Following Shaik's method, we have done further DFT calculations in which two THF molecules are included around the Fe center for all the molecules containing the iron atom in the whole catalytic process. All equilibrium structures are fully optimized in the gas phase. Then, the C-PCM polarizable conductor calculation model with the UFF radii is applied to calculate the solvation effects.

The fully optimized structures in the gas phase of the reactant **CA-2THF** and the intermediates **IN1−2THF** and **IN2−2THF** are shown in Figure 8, and the fully optimized structures in the gas phase of **D1−2THF**, **IN3−2THF**, and **D3−2THF** are shown in Figure 9. It can be seen that most of the structures do not change much, compared to those shown in Figures 2 and 3.

The bonding distance of Fe−Cl in the intermediate **IN2** increases from the previous 2.30 Å (see Figure 2) to 2.42 Å (see Figure 8), which means the interaction when two THF molecules are coordinated to the iron center favors the dissociation of molecule **D2**, [Cl−Mg−Br], leaving the iron center to form **D1**. This conclusion agrees with the previous

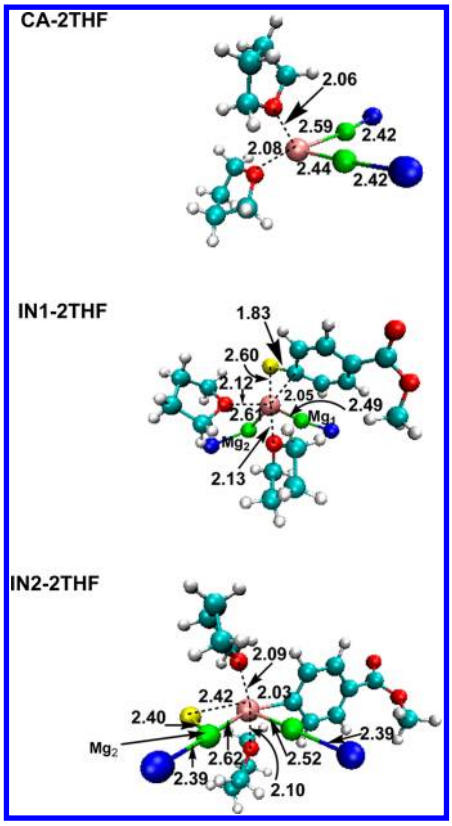

Figure 8. Fully optimized structures of the reactant and intermediates **CA-2THF**, **IN1−2THF**, and **IN2−2THF**. The unit of the distances is Å (C, cyan; O, red; Fe, pink; Mg,: green; Br, blue; Cl, yellow).

discussion about the solvation effect for ΔG_{sol} (**IN2** → **D1**) using the C-PCM method.

The calculated values of Gibb's free energy ΔG without or with two THF molecules in the gas phase, ΔG_g (no THF) and ΔG_g (2THF), and that of them in the THF solvent using C-PCM method, ΔG_{sol} (no THF) and ΔG_{sol} (2THF), are listed in columns 2−5 of Table 1, respectively. The unit of the energy is kcal/mol.

It can be seen that the differences between ΔG_g (no THF) and ΔG_g (2THF) are small for the processes (a) **CA** + **R1** → **IN1**, (b) **IN1** → **IN2**, (c) **IN2** → **D1**, and (d) **D1** → **IN3**, which means the energy calculations in the gas phase for the model without or with two THF molecules are not affected for the processes of a−d. However, the differences between ΔG_g (no THF) and ΔG_g (2THF) are large for the processes of (e) **IN3** → **D3** and (f) **D3** → **CA** + **D4**. According to the data in Table 1, the calculated Gibb's free energy ΔG_g (2THF) of **D3** is −55.54 kcal/mol based on the sum of the energies of **R1** and **CA** set as the zero of energy. This value is 13.60 kcal/mol higher than that of **D3** without two THF molecules in the gas phase (−69.14 kcal/mol, see Figure 7). So the interaction between **D3** and two THF molecules would lower the activation energy for the process of reductive elimination of **D3** to form the final product **D4**. This conclusion is in keeping with that obtained from the solvent calculations. The energy barrier of **TS3** from **D3** to **D4** in THF solvent calculated using C-PCM method, ΔG_{sol} (no THF), is 28.13 kcal/mol, which is smaller than that of it in the gas phase, ΔG_g (no THF) (32.40 kcal/mol, see Figure 7).

However, it can be seen that, from columns 4−5 of Table 1, the values of ΔG_{sol} (no THF) and ΔG_{sol} (2THF) calculated

dx.doi.org/10.1021/jp3045498 | J. Phys. Chem. A 2013, 117, 756−764

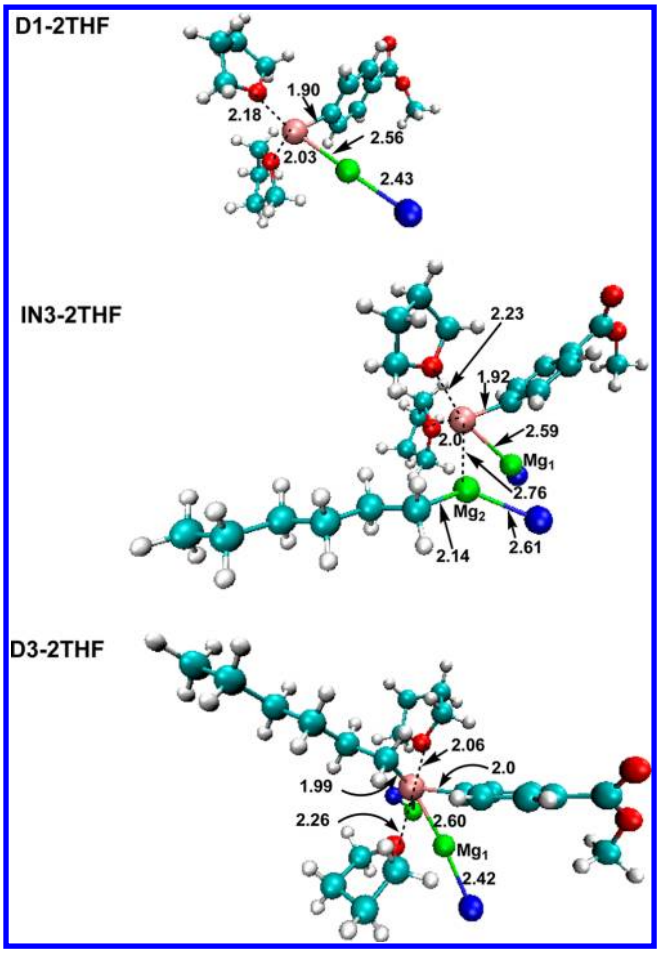

Figure 9. Fully optimized structures of the intermediates **D1**−**2THF**, **IN3**−**2THF**, and **D3**−**2THF**. The unit of the distances is Å (C, cyan; O, red; Fe, pink; Mg, green; Br, blue; Cl, yellow).

Table 1. Calculated Values of Gibb's Free Energy ΔG without or with Two THF Molecules Included in the Structures in the Gas Phase, ΔG_g (no THF) and ΔG_g (2THF), Compared to Those in the Solvent THF Using C-PCM Method, ΔG_{sol} (no THF) and ΔG_{sol} (2THF); the Unit Is kcal/mol

processes	ΔG_g (no THF)	ΔG_g (2THF)	ΔG_{sol} (no THF)	ΔG_{sol} (2THF)
(a) **CA** + **R1** → **IN1**	−5.60	−3.42	−2.78	−2.42
(b) **IN1** → **IN2**	−69.76	−70.51	−67.76	−70.17
(c) **IN2** → **D1**	24.71	29.00	1.39	−2.90
(d) **D1** → **IN3**	−6.43	−10.40	13.53	12.99
(e) **IN3** → **D3**	−12.06	−0.21	−18.93	−16.55
(f) **D3** → **CA** + **D4**	14.56	0.97	1.09	5.59

from C-PCM method in THF solvent change little in the whole processes for the model without or with two THF molecules, respectively. This means it is appropriate to use the C-PCM method for our system. If the C-PCM method overestimated the solvation energies, there would be a much larger change between the values calculated including two THF molecules and those without the THF molecules as suggested by Shaik.[69] The C-PCM method had been widely used to study the solvation effect for transition metal-catalyzed cross-coupling reactions.[39,70] Espinet[70] used the C-PCM approach to study the solvation effect of the Stille cross-coupling reaction catalyzed by PdL_2 (L = PH_3 and AsH_3) with PhBr as the electrophile and CH_2═$CHSnMe_3$ as the nucleophile in THF solvent.

4. CONCLUSIONS

Iron-catalyzed cross-coupling reactions have supplied an indispensible class of reactions to form carbon−carbon and carbon−heteroatom bonds in modern synthesis because simple iron salts have turned out to be highly efficient, cheap, toxicologically benign, and environmentally friendly precatalysts. Our studies report the first theoretical investigation of [Fe(MgBr)$_2$] catalyzed cross-coupling reaction between aryl chlorides and alkylmagnesium bromide using density functional theory (DFT) calculations.

The full catalytic cycle includes three basic steps: (I) oxidation of [Fe(MgBr)$_2$] to obtain the middle product **D1**, [Ar−Fe(MgBr)], (II) addition to yield the middle product **D3**, [Ar−(hexyl)−Fe(MgBr)$_2$], and (III) reductive elimination to return to the catalyst **CA**, [Fe(MgBr)$_2$]. The energy barrier is lower (electronic energy ΔE is 18.2 kcal/mol) if *n*-hexylicmagnesium bromide **R2** attacks the intermediate **IN2** directly to form a new intermediate before the molecule **D2** [Cl−Mg−Br] dissociates to form the middle product **D1** than if **R2** attacks **D1** after the molecule **D2** [Cl−Mg−Br] dissociates from **IN2** (electronic energy ΔE is 35.91 kcal/mol). The solvation effect in this step of **D2** dissociating from **IN2** to form **D1** is significant (see Figure 7). The computed Gibb's free energies in THF solution ΔG_{sol} (**IN2** → **D1**) using C-PCM method is 1.39 kcal/mol, which is much smaller than that in the gas phase, ΔG_g (**IN2** → **D1**) (24.71 kcal/mol). The models without or with two THF molecules included around the Fe center for all the molecules containing iron atom in the whole catalytic processes do not affect the results of Gibb's free energies in solution THF, ΔG_{sol}, using the C-PCM method. The rate-limiting step in the whole catalytic cycle is the reductive elimination of **D3** to form **D4** when the catalyst **CA** is regenerated, where the electronic energy barrier ΔE is 29.74 kcal/mol in the gas phase and ΔG_{sol} is 28.13 kcal/mol in THF solvent using the C-PCM method.

■ ASSOCIATED CONTENT

Ⓢ Supporting Information

Detailed molecule coordinates of all optimized structures. This material is available free of charge via the Internet at http://pubs.acs.org.

■ AUTHOR INFORMATION

Corresponding Author

*E-mail: qinghua.ren@shu.edu.cn.

Notes

The authors declare no competing financial interest.

■ ACKNOWLEDGMENTS

This work is supported by Shanghai Leading Academic Discipline Project (J50101 and S30107) and Innovation funding of Shanghai University. Q.R. is thankful for the help of Professor Gabriel G. Balint-Kurti and Professor Jeremy N. Harvey of the University of Bristol.

■ REFERENCES

(1) Cahiez, G.; Duplais, C.; Buendia, J. Chemistry of Organomanganese(II) Compounds. *Chem. Rev.* **2009**, *109*, 1434−1476.

(2) Denmark, S. E.; Sweis, R. F. Fluoride-Free Cross-Coupling of Organosilanols. *J. Am. Chem. Soc.* **2001**, *123*, 6439−6440.
(3) Alberico, D.; Scott, M. E.; Lautens, M. Aryl−Aryl Bond Formation by Transition-Metal-Catalyzed Direct Arylation. *Chem. Rev.* **2007**, *107*, 174−238.
(4) Diederich, F.; Stang, P. J. *Metal-Catalyzed Cross-Coupling Reactions*; Wiley-VCH: Weinheim, Germany, 1998.
(5) Hassan, J.; Sevignon, M.; Gozzi, C.; Schulz, E.; Lemaire, M. Aryl−Aryl Bond Formation One Century after the Discovery of the Ullmann Reaction. *Chem. Rev.* **2002**, *102*, 1359−1469.
(6) Beller, M.; Bolm, C *Transition Metals for Organic Synthesis*; Wiley-VCH: Weinheim, Germany, 2004.
(7) Miyaura, N.; Suzuki, A. Palladium-Catalyzed Cross-Coupling Reactions of Organoboron Compounds. *Chem. Rev.* **1995**, *95*, 2457−2483.
(8) Negishi, E. A Genealogy of Pd-Catalyzed Cross-Coupling. *J. Organomet. Chem.* **2002**, *653*, 34−40.
(9) Suzuki, A. Recent Advances in the Cross-Coupling Reactions of Organoboron Derivatives with Organic Electrophiles. *J. Organomet. Chem.* **1999**, *576*, 147−168.
(10) Wolfe, J. P.; Wagaw, S.; Marcoux, J. F.; Buchwald, S. L. Rational Development of Practical Catalysts for Aromatic Carbon−Nitrogen Bond Formation. *Acc. Chem. Res.* **1998**, *31*, 805−818.
(11) Negishi, E. *Handbook of Organopalladium Chemistry for Organic Synthesis*; Wiley: New York, 2002.
(12) Tsuji, J. *Palladium Reagents and Catalysts: Innovations in Organic Synthesis*; Wiley: New York, 1996.
(13) Selander, N.; Szabo, K. J. Catalysis by Palladium Pincer Complexes. *Chem. Rev.* **2011**, *111*, 2048−2076.
(14) Rosen, B. M.; Quasdorf, K. W.; Wilson, D. A.; Zhang, N.; Resmerita, A. M.; Grag, N. K.; Percec, V. Nickel-Catalyzed Cross-Couplings Involving Carbon−Oxygen Bonds. *Chem. Rev.* **2011**, *111*, 1346−1416.
(15) Bauer, E. B. Recent Advances in Iron Catalysis in Organic Synthesis. *Curr. Org. Chem.* **2008**, *12*, 1341−1369.
(16) Bolm, C.; Legros, J.; Paih, J. L.; Zani, L. Iron-Catalyzed Reactions in Organic Synthesis. *Chem. Rev.* **2004**, *104*, 6217−6254.
(17) Czaplik, W. M.; Mayer, M.; Cvengros, J.; von Wangelin, A. J. Coming of Age: Sustainable Iron-Catalyzed Cross-Coupling Reactions. *ChemSusChem* **2009**, *2*, 396−417.
(18) Sherry, B. D.; Furstner, A. The Promise and Challenge of Iron-Catalyzed Cross Coupling. *Acc. Chem. Res.* **2008**, *41*, 1500−1511.
(19) Kochi, J. K. Electron-Transfer Mechanisms for Organometallic Intermediates in Catalytic Reactions. *Acc. Chem. Res.* **1974**, *7*, 351−360.
(20) Tamura, M.; Kochi, J. K. Vinylation of Grignard Reagents Catalysis by Iron. *J. Am. Chem. Soc.* **1971**, *93*, 1487−1489.
(21) Furstner, A.; Leitner, A. Iron-Catalyzed Cross-Coupling Reactions of Alkyl-Grignard Reagents with Aryl Chlorides, Tosylates, and Triflates. *Angew. Chem., Int. Ed.* **2002**, *41*, 609−612.
(22) Furstner, A.; Leitner, A.; Mendez, M.; Krause, H. Iron-Catalyzed Cross-Coupling Reactions. *J. Am. Chem. Soc.* **2002**, *124*, 13856−13863.
(23) Bi, H. P.; Chen, W. W.; Liang, Y. M.; Li, C. J. A Novel Iron-Catalyzed Decarboxylative Csp^3−Csp^2 Coupling of Proline Derivatives and Naphthol. *Org. Lett.* **2009**, *11*, 3246−3249.
(24) Correa, A.; Mancheno, O. G.; Bolm, C. Iron-Catalysed Carbon−Heteroatom and Heteroatom−Heteroatom Bond Forming Processes. *Chem. Soc. Rev.* **2008**, *37*, 1108−1117.
(25) Furstner, A.; Majima, K.; Martin, R.; Krause, H.; Kattnig, E.; Goddard, R.; Lehmann, C. W. A Cheap Metal for a "Noble" Task: Preparative and Mechanistic Aspects of Cycloisomerization and Cycloaddition Reactions Catalyzed by Low-Valent Iron Complexes. *J. Am. Chem. Soc.* **2008**, *130*, 1992−2004.
(26) Furstner, A.; Martin, R. Advances in Iron Catalyzed Cross Coupling Reactions. *Chem. Lett.* **2005**, *34*, 624−629.
(27) Furstner, A.; Martin, R.; Krause, H.; Seidel, G.; Goddard, R.; Lehmann, C. W. Preparation, Structure, and Reactivity of Non-stabilized Organoiron Compounds. Implications for Iron-Catalyzed Cross Coupling Reactions. *J. Am. Chem. Soc.* **2008**, *130*, 8773−8787.
(28) Noda, D.; Sunada, Y.; Hatakeyama, T.; Nakamura, M.; Nagashima, H. Effect of TMEDA on Iron-Catalyzed Coupling Reactions of ArMgX with Alkyl Halides. *J. Am. Chem. Soc.* **2009**, *131*, 6078−6079.
(29) Phua, P. H.; Lefort, L.; Boogers, J. A. F.; Tristany, M.; de Vries, J. G. Soluble Iron Nanoparticles As Cheap and Environmentally Benign Alkene and Alkyne Hydrogenation Catalysts. *Chem. Commun.* **2009**, 3747−3749.
(30) Scheiper, B.; Bonnekessel, M.; Krause, H.; Furstner, A. Selective Iron-Catalyzed Cross-Coupling Reactions of Grignard Reagents with Enol Triflates, Acid Chlorides, and Dichloroarenes. *J. Org. Chem.* **2004**, *69*, 3943−3949.
(31) Amatore, C.; Azzabi, M.; Jutand, A. Rates and Mechanism of the Reversible Oxidative Addition of (*Z*)- and (*E*)-1,2-Dichloroethylene to Low-Ligated Zerovalent Palladium. *J. Am. Chem. Soc.* **1991**, *113*, 1670−1677.
(32) Cardenas, D. J.; Echavarren, A. M. Mechanistic Aspects of C−C Bond Formation Involving Allylpalladium Complexes: the Role of Computational Studies. *New J. Chem.* **2004**, *28*, 338−347.
(33) Yamamoto, A. Organotransition-Metal Chemistry: Past Development and Future Outlook. *J. Organomet. Chem.* **2000**, *600*, 159−167.
(34) Alvarez, R.; Perez, M.; Faza, O. N.; de Lera, A. R. Associative Transmetalation in the Stille Cross-Coupling Reactions to Form Dienes: Theoretical Insights into the Open Pathway. *Organometallics* **2008**, *27*, 3378−3389.
(35) Lakmini, H.; Ciofini, I.; Jutand, A.; Amatore, C.; Adamo, C. Pd-Catalyzed Homocouplimg Reactions of Arylboronic Acid: Insights from Density Functional Theory. *J. Phys. Chem. A* **2008**, *112*, 12896−12903.
(36) Li, Z.; Fu, Y.; Guo, Q. X.; Liu, L. Theoretical Study on Monoligated Pd-Catalyzed Cross-Coupling Reactions of Aryl Chlorides and Bromides. *Organometallics* **2008**, *27*, 4043−4049.
(37) Sugiyama, A.; Ohnishi, Y. Y.; Nakaoka, M.; Nakao, Y.; Sato, H.; Sakaki, S.; Nakao, Y.; Hiyama, T. Why Does Fluoride Anion Accelerate Transmetalation between Vinylsilane and Palladium(II)−Vinyl Complex? Theoretical Study. *J. Am. Chem. Soc.* **2008**, *130*, 12975−12985.
(38) Yamamoto, Y.; Takada, S.; Miyaura, N.; Iyama, T.; Tachikawa, H. γ-Selective Cross-Coupling Reactions of Potassium Allyltrifluoroborates with Haloarenes Catalyzed by a Pd(0)/D-*t*-BPF or Pd(0)/Josiphos ((*R*,*S*)-CyPF-*t*-Bu) Complex: Mechanistic Studies on Transmetalation and Enantioselection. *Organometallics* **2009**, *28*, 152−160.
(39) Li, Z.; Zhang, S. L.; Fu, Y.; Guo, Q. X.; Liu, L. Mechanism of Ni-Catalyzed Selective C−O Bond Activation in Cross-Coupling of Aryl Esters. *J. Am. Chem. Soc.* **2009**, *131*, 8815−8823.
(40) McCarren, P. R.; Liu, P.; Cheong, P. H. Y.; Jamison, T. F.; Houk, K. N. Mechanism and Transition-State Structures for Nickel-Catalyzed Reductive Alkyne−Aldehyde Coupling Reactions. *J. Am. Chem. Soc.* **2009**, *131*, 6654−6655.
(41) Li, T.; Jones, W. D. DFT Calculations of the Isomerization of 2-Methyl-3-butenenitrile by [Ni(bisphosphine)] in Relation to the DuPont Adiponitrile Process. *Organometallics* **2011**, *30*, 547−555.
(42) Torres-Nieto, J.; Brennessel, W. W.; Jones, W. D.; Garcia, J. J. Mechanistic Insights on the Hydrodesulfurization of Biphenyl-2-thiol with Nickel Compounds. *J. Am. Chem. Soc.* **2009**, *131*, 4120−4126.
(43) Yang, J. Y.; Bullock, R. M.; Shaw, W. J.; Twamley, B.; Fraze, K.; DuBois, M. R.; DuBois, D. L. Mechanistic Insights into Catalytic H_2 Oxidation by Ni Complexes Containing a Diphosphine Ligand with a Positioned Amine Base. *J. Am. Chem. Soc.* **2009**, *131*, 5935−5945.
(44) Joseph, J.; RajanBabu, T. V.; Jemmis, E. D. A Theoretical Investigation of the Ni(II)-Catalyzed Hydrovinylation of Styrene. *Organometallics* **2009**, *28*, 3552−3566.
(45) Smith, R. S.; Kochi, J. K. Mechanistic Studies of Iron Catalysis in the Cross Coupling of Alkenyl Halides and Grignard Reagents. *J. Org. Chem.* **1976**, *41*, 502−509.
(46) Takacs, J. M.; Anderson, L. G.; Madhavan, G. V. B.; Creswell, M. W.; Seely, F. L.; Devroy, W. F. Transition-Metal-Catalyzed Carbon−Carbon Bond Forming Reactions: Regio- and Chemo-

selective Iron(0)-Catalyzed Diene to Olefin Cross-Coupling Reactions. *Organometallics* **1986**, *5*, 2395−2398.
(47) Bogdanovic, B.; Schwickardi, M. Transition Metal Catalyzed Preparation of Grignard Compounds. *Angew. Chem., Int. Ed.* **2000**, *39*, 4610−4612.
(48) Kleimark, J.; Hedstrom, A.; Larsson, P. F.; Johansson, C.; Norrby, P. Mechanistic Investigation of Iron-Catalyzed Coupling Reactions. *ChemCatChem* **2009**, *1*, 152−161.
(49) Czaplik, W. M.; Mayer, M.; von Wangelin, A. J. Iron-Catalyzed Reductive Aryl−Alkenyl Cross-Coupling Reactions. *ChemCatChem* **2011**, *3*, 135−138.
(50) Shirakawa, E.; Ikeda, D.; Masui, S.; Yoshida, M.; Hayashi, T. Iron−Copper Cooperative Catalysis in the Reactions of Alkyl Grignard Reagents: Exchange Reaction with Alkenes and Carbometalation of Alkynes. *J. Am. Chem. Soc.* **2012**, *134*, 272−279.
(51) Gulak, S.; von Wangelin, A. J. Chlorostyrenes in Iron-Catalyzed Biaryl Coupling Reactions. *Angew. Chem., Int. Ed.* **2012**, *51*, 1357−1361.
(52) Becke, A. D. Density-Functional Exchange-Energy Approximation with Correct Asymptotic Behavior. *Phys. Rev. A* **1988**, *38*, 3098−3100.
(53) Becke, A. D. Density-Functional Thermochemistry. III. The Role of Exact Exchange. *J. Chem. Phys.* **1993**, *98*, 5648−5652.
(54) Hertwig, R. H.; Koch, W. On the Parameterization of the Local Correlation Functional. What is Becke-3-LYP? *Chem. Phys. Lett.* **1997**, *268*, 345−351.
(55) Lee, C. T.; Yang, W. T.; Parr, R. G. Development of the Colle-Salvetti Correlation-Energy Formula into a Functional of the Electron Density. *Phys. Rev. B* **1988**, *37*, 785−789.
(56) Stephens, P. J.; Devlin, F. J.; Chabalowski, C. F.; Frisch, M. J. Ab Initio Calculation of Vibrational Absorption and Circular Dichroism Spectra Using Density Functional Force Fields. *J. Phys. Chem.* **1994**, *98*, 11623−11627.
(57) Vosko, S. H.; Wilk, L.; Nusair, M. Accurate Spin-Dependent Electron Liquid Correlation Energies for Local Spin Density Calculations: a Critical Analysis. *Can. J. Phys.* **1980**, *58*, 1200−1211.
(58) Krishnan, R.; Binkley, J. S.; Seeger, R.; Pople, J. A. Self-Consistent Molecular Orbital Methods. XX. A Basis Set for Correlated Wave Functions. *J. Chem. Phys.* **1980**, *72*, 650−4.
(59) McLean, A. D.; Chandler, G. S. Contracted Gaussian Basis Sets for Molecular Calculations. I. Second Row Atoms, Z = 11−18. *J. Chem. Phys.* **1980**, *72*, 5639−5648.
(60) Andrae, D.; Haussermann, U.; Dolg, M.; Stoll, H.; Preuss, H. Energy-Adjusted ab Initio Pseudopotentials for the Second and Third Row Transition Elements. *Theor. Chim. Acta* **1990**, *77*, 123−141.
(61) Cossi, M.; Rega, N.; Scalmani, G.; Barone, V. Energies, Structures, and Electronic Properties of Molecules in Solution with the C-PCM Solvation Model. *J. Comput. Chem.* **2003**, *24*, 669−681.
(62) Frisch, M. J.; et al. *Gaussian 03*, version 01; Gaussian, Inc.: Wallingford, CT, 2004.
(63) Castejon, H.; Wiberg, K. B. Solvent Effects on Methyl Transfer Reactions. 1. The Menshutkin Reaction. *J. Am. Chem. Soc.* **1999**, *121*, 2139−2146.
(64) Perng, B. C.; Newton, M. D.; Raineri, F. O.; Friedman, H. L. Energetics of Charge Transfer Reactions in Solvents of Dipolar and Higher Order Multipolar Character 0.1. Theory; 2. Results. *J. Chem. Phys.* **1996**, *104*, 7153−7176 and 7177−7204.
(65) Najafi, M.; Zahedi, M.; Klein, E. DFT/B3LYP Study of the Solvent Effect on the Reaction Enthalpies of Homolytic and Heterolytic O−H Bond Cleavage in Mono-Substituted Chromans. *Comput. Theor. Chem.* **2011**, *978*, 16−28.
(66) Schubert, G.; Papai, I. Acrylate Formation via Metal-Assisted C−C Coupling between CO_2 and C_2H_4: Reaction Mechanism As Revealed from Density Functional Calculations. *J. Am. Chem. Soc.* **2003**, *125*, 14847−14858.
(67) Senn, H. M.; Ziegler, T. Oxidative Addition of Aryl Halides to Palladium(0) Complexes: A Density-Functional Study Including Solvation. *Organometallics* **2004**, *23*, 2980−2988.
(68) Kozuch, S.; Shaik, S.; Jutand, A.; Amatore, C. Active Anionic Zero-Valent Palladium Catalysts: Characterization by Density Functional Calculations. *Chem.—Eur. J.* **2004**, *10*, 3072−3080.
(69) Kozuch, S.; Amatore, C.; Jutand, A.; Shaik, S. What Makes for a Good Catalytic Cycle? A Theoretical Study of the Role of an Anionic Palladium(0) Complex in the Cross-Coupling of an Aryl Halide with an Anionic Nucleophile. *Organometallics* **2005**, *24*, 2319−2330.
(70) Nova, A.; Ujaque, G.; Maseras, F.; Liedos, A.; Espinet, P. A Critical Analysis of the Cyclic and Open Alternatives of the Transmetalation Step in the Stille Cross-Coupling Reaction. *J. Am. Chem. Soc.* **2006**, *128*, 14571−14578.